Electrochemical and thermodynamic study of the inhibitory effect of triglycidyl ether tripropoxy triazine (TGETPT) on the corrosion of carbon steel E24 in 1 M hydrochloric acid medium

M.E. Ansar,[1]* R. Hsissou,[2] B.E. Ibrahimi,[3] A.A. Addi,[3] A. Molhi,[1] M. Damej,[1] S. El Hajjaji[4] and M. Benmessaoud[1]

[1]*Environment, Materials and Sustainable Development Team – CERNE2D, High School of Technology, Mohammed V University in Rabat, Morocco*
[2]*Laboratory of Agro Resources. Polymers and Process Engineering (LAPPE). Team of Organic and Polymer Chemistry (TOCP). Faculty of Sciences, Ibn Tofail University in Kenitra, Morocco*
[3]*Team of Physical Chemistry and Environment, Faculty of Science, Ibn Zohr University in Agadir, Morocco*
[4]*Laboratory of Spectroscopy, Molecular Modelling Materials, Nanomaterial Water and Environment –CERNE2D, Faculty of Sciences, Mohammed V University in Rabat, Morocco*
**E-mail: med.elmahdi.ansar@gmail.com*

Abstract

Corrosion is of importance to multidisciplinary study groups as it includes materials science, chemistry, physics, metallurgy, and chemical engineering. Corrosion is induced by an environment's chemical and electrochemical impact on metals and alloys. The objective of this work is to investigate the corrosion inhibition behavior of triglycidyl ether tripropoxy triazine (TGETPT) on of E24 steel in 1 M HCl. This study was carried out by electrochemical methods (polarization curves and electrochemical impedance spectroscopy). The polarization curves indicate that the inhibition mechanism is mainly acting as mixed-type inhibitor, and the corrosion rate of E24 in 1 M HCl is reduced 81.6% at inhibitor concentration of 10^{-3} M. The electrochemical impedance diagrams show that the inhibition is a process of charge transfer on a heterogeneous surface for all tested TGETPT concentrations. Scanning electron microscope micrographs demonstrated that the epoxy prepolymer could effectively block the acid attack by physical adsorption on the surface of the carbon steel, the high correlation coefficient and low Standard Deviation and low Sum of Squares value gave the best fit for Langmuir isotherm. The effect of temperature on the corrosion behaviour with the addition of TGETPT was studied in the temperature range 293–323 K. The theoretical investigations through DFT-based quantum chemical calculations and molecular dynamics simulations are in good agreement with the experimental results.

Received: March 17, 2023. Published: August 20, 2023 doi: 10.17675/2305-6894-2023-12-3-16

Keywords: *corrosion inhibition, polarization, impedance spectroscopy, E24, DFT.*

1. Introduction

Nature attempts to convert metals back into their natural state as soon as they are extracted from their ores. As a result, metals react with the aggressive species in the surrounding environment, forming compounds such as metallic chlorides, carbonate oxides, sulfides, and so on [1]. Aqueous metallic corrosion is the most common type of corrosion, in which the material is a metal or an alloy and the environment is an aqueous solution. This natural occurrence is referred to as "metallic corrosion". Corrosion manifests itself in a variety of ways in our daily lives. For instance, holes in automobiles, reddish-orange spots on metal surfaces, brown murky water taps, corroded nails, leaking hot water tanks, and so on [2]. To reduce steel corrosion, corrosion inhibitors are often added to the acidizing solution. Studies have shown that organic compounds containing polar functional groups, π-electrons, and heteroatoms such as S, O, and/or N, can be effective corrosion inhibitors [3–9]. These inhibitors work by attaching themselves to the steel surface, creating a protective layer that reduces the corrosion reaction. This attachment can occur through physical, chemical, or physicochemical adsorption [10–12].

Pickling treatments, acid cleaning operations, and oil well acidizing for steel are all common uses for acid solutions of various concentrations, these operations lead to the increased corrosion process, as hydrogen ions are released in the acidic solution, which acts as a cathode, increasing the dissolution of the metal [13, 14]. In order to reduce this problem, corrosion inhibitors are commonly used [15, 16].

An inhibitor is a chemical substance that is introduced to the medium in tiny amounts to limit the rate of corrosion of materials. It can be used to either protect the part permanently (requiring careful installation) or temporarily (especially when the part is particularly sensitive to corrosion or when it is exposed to a very aggressive environment) [17–19]. Inhibitory compounds can work through several methods, giving them varied inhibitory performance depending on the research medium [20–22].

Recently, computer modeling, mainly calculation based on DFT and molecular dynamics simulations, have been led to a good understanding of the inhibition mechanism of a given corrosion inhibitor, in this regard, both computational tools have been used in the current work to explain and substantiate the experimental results [23–25].

The objective of this study is to evaluate the inhibition properties of epoxy polymer TGETPT on the corrosion of E24 steel in a 1 M hydrochloric acid solution. The electrochemical analysis reveals that the TGETPT compound hinders the corrosion process of E24 steel by generating a protective film on its surface. SEM/EDX analysis further supports these findings. Theoretical computations are often utilized to obtain a comprehensive understanding of the adsorption behavior of inhibitors at the molecular level, including their adsorption sites, adsorption energy, and adsorption geometry on the metal surface.

2. Material and Methods

2.1. Preparation of metal and corrosive medium

The metal used in this study is E24 and its chemical composition is listed in Table 1. The specimens selected had a circular surface area of 1 cm^2. Before each test, the specimen was polished with sandpapers of (Grade: 600, 1200, and 1500), rinsed with distilled water and alcohol, and then dried in air.

Table 1. The chemical compositions of E24.

C%	Si%	P%	S%	Ti%	Co %	Cr%	Mn%	Fe%
0.11	0.24	0.021	0.16	0.011	0.009	0.077	0.47	99.046

The corrosive medium is a 1 M HCl solution, which was made from distilled water and a commercial solution of hydrochloric acid (37%). The inhibitor (TGETPT) dosages utilized ranged from 0.05 to 1 mM.

2.2. Synthesis of triglycidyl ether tripropoxy triazine (TGETPT) heterocyclic epoxy resin

The novelty heterocyclic epoxy resin namely triglycidyl ether tripropoxy triazine (TGETPT) was synthesized through condensation reaction [26, 27]. Firstly, we condensed $5.374 \cdot 10^{-3}$ mol of propane-1,3-diol (purity of 98%) with $2.876 \cdot 10^{-3}$ mol of 2,4,6-trichloro-1,3,5-triazine (purity of 98%) using ethanol as solvent under magnetic stirring for 24 h at 80°C. Then, we added $6.953 \cdot 10^{-3}$ mol of epichlorohydrin (purity of 99%) to the reaction mixture under magnetic stirring for 4 h at 70°C. Besides, we added $8.235 \cdot 10^{-3}$ mol of triethylamine (purity of 99.5%) as a basis under magnetic stirring for 3 h at 40°C (Scheme 1). Additionally, the excess ethanol was removed by using the rotary evaporator.

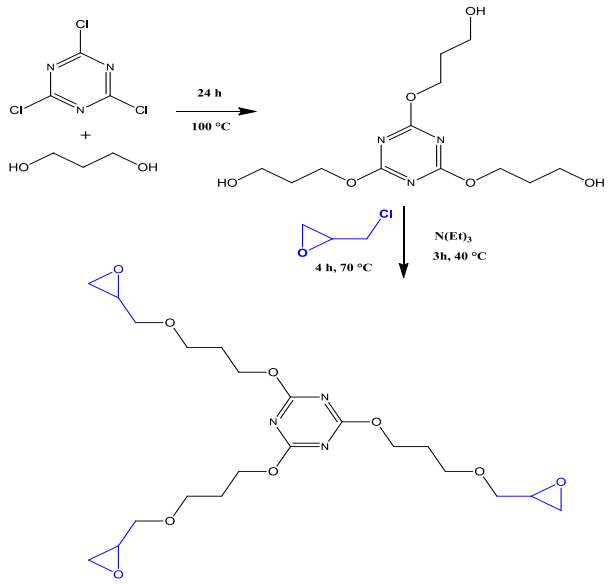

Scheme 1. Reaction of synthesis of TGETPT.

2.3. Electrochemical measurements

The electrochemical investigation was done utilizing Volta Master software driven potentiostat PGZ 100. A three-electrode cell with a carbon steel (E24) working electrode, a saturated calomel reference electrode, and a platinum (Pt) electrode serving as a counter were used for the experiments. Before all the electrochemical analysis, the working electrode was plunged into a corrosive solution for 60 min in a quasi-stationary condition at an open circuit potential. With a scanning rate of 1 mV/sec around an open-circuit potential, polarization curves were obtained between −800 and −100 mV. In the Nyquist plot, the spectroscopy with electro-chemical impedance (EIS) was provided in the frequency range from 100 kHz to 10 mHz at ambient temperature.

The inhibition effectiveness (*IE*%) for polarization curves was determined by the following equation [28]:

$$IE\% = \frac{i^0 - i^{\text{inh}}}{i^0} \cdot 100 \tag{1}$$

where i^0 is current densities uninhibited and, i^{inh} is corrosion current densities inhibited with various concentrations of TGETPT.

The inhibition efficiency *IE*% of electrochemical impedance spectroscopy (EIS) plots was determined by the equation below [29].

$$IE\% = \frac{R_{\text{p}}^{\text{inh}} - R_{\text{p}}^0}{R_{\text{p}}^{\text{inh}}} \cdot 100 \tag{2}$$

where $R_{\text{p}}^{\text{inh}}$ and R_{p}^0 indicate the polarization resistance inhibited and polarization resistance uninhibited with diverse concentrations of TGETPT, respectively.

2.4. Scanning electron microscopy/energy dispersive X-ray analysis

Closer examination using scanning electron microscopy (SEM) enables the selection of surfaces to be analyzed based on several microstructural criteria. The micrograph of the E24 surface was examined after 20 hours of immersion in the acid medium without and with TGETPT, and energy dispersive X-ray (EDX) was applied for chemical composition characterization [30].

2.5. DFT

Density functional theory (DFT) calculations were performed using the DMol3 module included in Material Studio 6.0 software to investigate both the local and global reactivity of tested inhibitors and their involvement in the inhibition process. The geometry optimization of the inhibitor molecule, as well as the calculation of different associated quantum chemical parameters, were done employing generalized gradient approximation (GGA) functional of Becke exchange plus Lee–Yang–Parr correlation (BLYP) [31]. Double numerical plus polarization (DNP) version 3.5 served as the basis set. To consider the effect of an aqueous solution, the COSMO method was used [32].

2.6. Dynamic molecular findings

To investigate the adsorption behavior of tested TGETPT on the E24 surface, molecular dynamic simulation was performed for 50 ps at 298 K setting 1 fs as time step and using Berendsen thermostat. To model the aqueous phase, $200H_2O+5H_3O^+ +5Cl^-$ composition was used with one inhibitor molecule. The molecular modelling was carried out on Fe(110) face in a simulation box of 27.31 Å×27.31 Å×68.11 Å dimensions with 60 Å as a sufficient vacuum region [33]. The calculations were conducted under periodic boundary conditions (PBC) and using COMPASS force field [34]. To compute electrostatic and Van der Waals interactions, Ewald and atom-based summation methods are used, respectively [35]. The adsorption energy (E_{ads}) of tested inhibitor molecules is calculated using the following formulate:

$$E_{total} - \left(E_{inh} - E_{sol+met}\right) \quad (3)$$

where E_{total} is the energy of the full system, E_{inh} is the energy of TGETPT and $E_{sol+met}$ is the energy without inhibitor [36].

3. Results and Discussion

3.1. FTIR analysis

Triglycidyl ether tripropoxy triazine (TGETPT) heterocyclic epoxy resin synthesized was characterized and confirmed through utilizing the Fourier transform infrared (FTIR) spectroscopy of BRUKER type to determine and identify the different functional groups. FTIR spectrum of novelty TGETPT is illustrated in Figure 1.

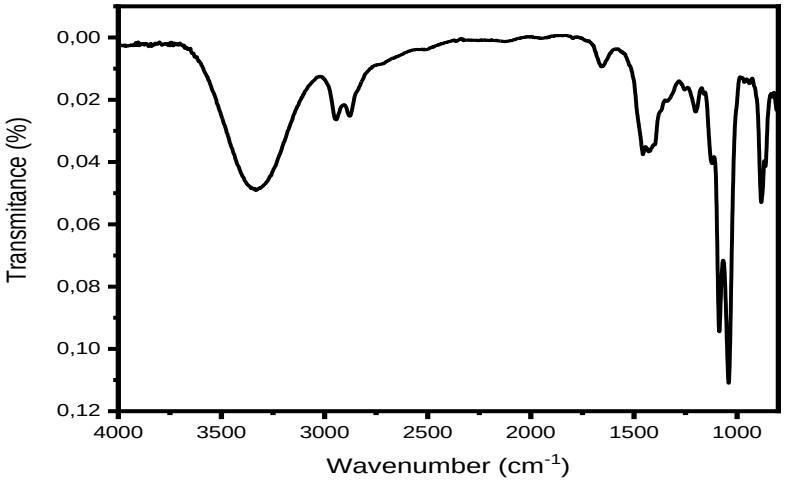

Figure 1. IR spectra of synthesized TGETPT.

The absorption band assigned at 3260 cm^{-1} is attributed to the stretching vibrations of the alcohol function (–OH) of the unclosed oxirane system of epoxy resin elaborated. Furthermore, the absorption bands situated at 2980 and 2965 cm^{-1} correspond to the stretching vibration of aliphatic methylene $(CH_2)_3$. Then, the absorption band located at 1485 is attributed to the C=N of the heterocyclic compound. In addition, the absorption band that appeared at 1030 cm^{-1} can be attributed to the unsymmetrical stretching vibration of the C–O–C ether function. Also, the presence of the epoxide group is indicated by the characteristic absorption band at 850 cm^{-1}, which is attributed to the oxirane system stretching vibration.

3.2. Electrochemical measurements

3.2.1. Open circuit potential

Figure 2 depicts the open circuit potential in the absence and presence of TGETPT at various concentrations after immersing carbon steel E24 in a 1 M HCl solution for 3600 s.

The OCP curves in different concentrations of TGETPT show that open circuit potentials have been formed [37]. Furthermore, parallel OCP *vs* time curves shows that the surface accumulated oxide layer has been eliminated, and the adsorption of the inhibitor molecules has been accomplished in less than 20 minutes. Similarly, the deviation of the TGETPT open circuit potential curves from the blank curve might imply a mixed inhibition of corrosion [38].

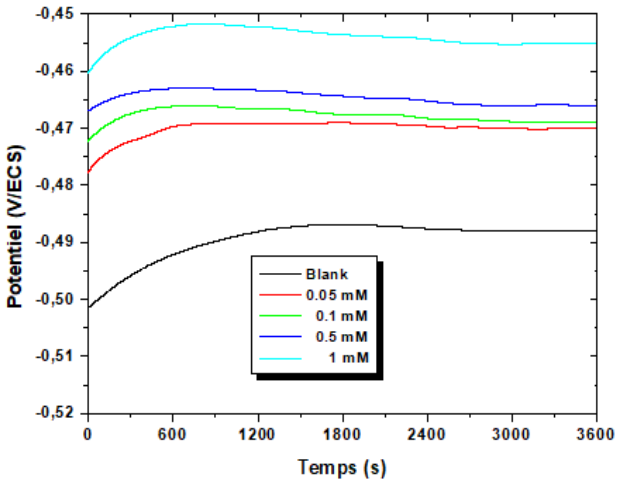

Figure 2. Evolution of E_{corr} of E24 in 1 M HCl solution of TGETPT at 293 K.

3.2.2. Potentiodynamic polarization measurements

The potentiodynamic polarization curves were obtained after E_{ocp} reaches a stable state (SCE), and the results are shown in Figure 3.

The addition of TGETPT, shifted both the cathodic and anodic curves to a decreased current density, resulting in a significant decrease in the rate of anodic metal oxidation and cathodic reduction of H^+ ions at all tested concentrations [39]. Moreover, the displacement in E_{corr} with the addition of TGETPT towards a positive direction (most noble), confirmed the open circuit potential results. This finding suggests that the TGETPT polymer and the E24 surface have significant interactions.

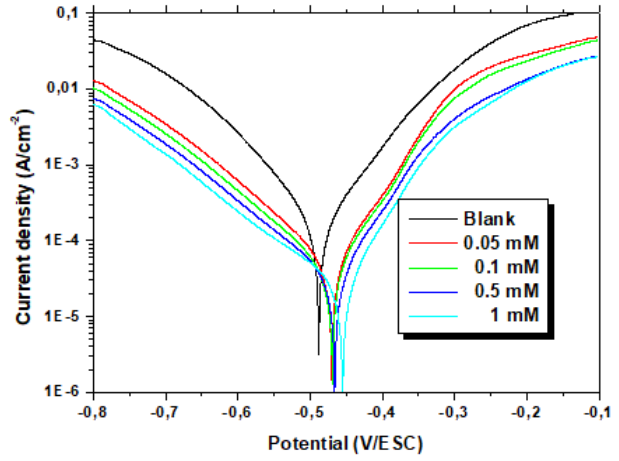

Figure 3. Potentiodynamic polarization curves of E24 steel in 1 M HCl in the absence and in the presence of different concentrations of TGETPT at 293 K.

Table 1 shows the electrochemical corrosion kinetic parameters corrosion potential (E_{corr}) and corrosion current density (i_{corr}) derived from the extrapolation of cathodic polarization curves. The corrosion current density (i_{corr}) decreased as inhibitor adsorption

increased and the inhibition efficiency increases as the inhibitor concentration increases, as calculated by the i_{corr} values.

The various concentrations of the TGETPT were tested to reduce the values of the Tafel slope (β_c) and (β_a) compared to hydrochloric acid alone. The results suggested that adding the inhibitor to the electrolyte affected the mechanism of hydrogen reduction [40, 41]. Also, the inhibitory efficiency of the TGETPT inhibitor reached 86% at 10^{-3} M. The TGETPT polymer is rich in electrons, and the electronic density of these letters increases. This facilitated its adsorption on E24 carbon steel, thus increasing inhibitory efficiency [42].

Table 1. Electrochemical parameters of E24 steel at various concentrations of TGETPT in 1 M HCl and corresponding inhibition efficiency *IE*%.

[TGETPT] mM	E_{corr} **(mV/Ag–AgCl)**	I_{corr} **(μA/cm²)**	$-\beta_c$ **(mV/dec)**	β_a **(mV/dec)**	***EI*** **(%)**
1 M	–488	174.8	94.7	93.3	–
0.05	–470	48.8	115.5	77.8	72.08
0.1	–469	38.93	122.8	77.3	77.73
0.5	–466	31.29	133.5	73.7	82.10
1	–455	24.37	149.9	65.3	86.06

3.2.3. Electrochemical impedance spectroscopy (EIS)

Transient electrochemical procedures, particularly electrochemical impedance spectroscopy (EIS), are capable to distinguish the elementary phenomena that are expected to emerge at the metal/solution interface based on their kinetics. EIS measurements are especially useful for understanding the mechanism of action of inhibitors, measuring the dielectric properties of the generated film, and tracking their evolution according to a variety of factors. It also allows for the explanation of the chemical or electrochemical processes that occur as a result of the formation of the films.

Impedance measurements were performed in this study to learn more about the corrosion inhibition mechanism of E24 submerged in 1 M HCl alone and in the presence of a tested inhibitor (TGETPT). The Nyquist and Bode plots for E24 without and with TGETPT are shown in Figure 4, and the electrochemical parameters derived from these curves are included in Table 2.

Demonstrating a striking resemblance in the impedance curve morphologies across all concentrations. According to this, an inhibitor effectively slows down corrosion processes while maintaining the corrosion mechanism [43]. This pattern leads one to believe that the inhibitory effect is produced by the steel surface's active corrosion sites being blocked by inhibitor molecules that have been adsorbed there [44, 45].

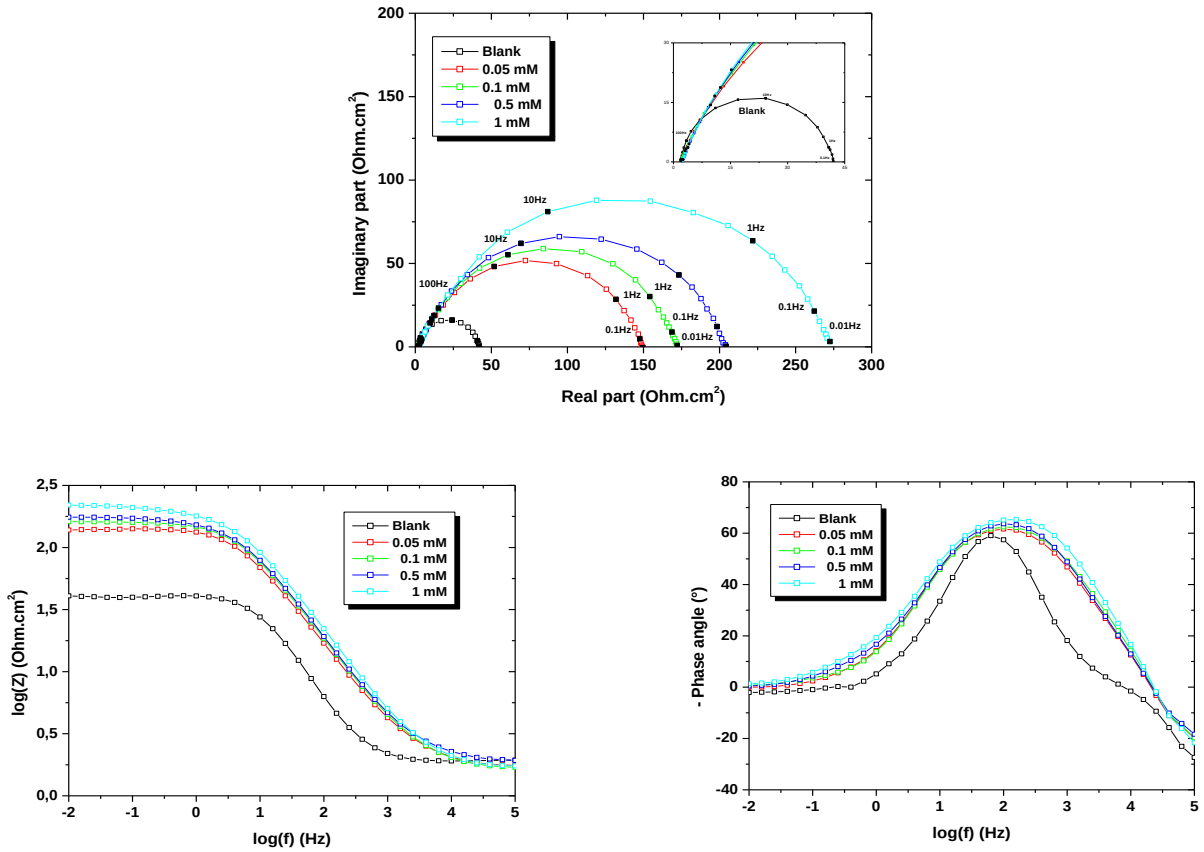

Figure 4. Nyquist, Bode, and phase angle diagrams for E24 steel in 1 M HCl without and with the different concentrations of TGETPT at 293 K.

Table 2. Electrochemical impedance parameters for corrosion of E24 steel in 1 M HCl without and with the different concentrations of TGETPT.

[TGETPT] (mM)	R_s ($\Omega \cdot cm^2$)	R_{ct} ($\Omega \cdot cm^2$)	CPE_{dl} ($\mu F \cdot cm^{-2}$)	E (%)	θ
0	1.920	39.67	401.1	–	–
0.05	2.574	147.5	120.87	71.85	0.7185
0.1	2.587	169.47	105.18	76.59	0.7659
0.5	2.411	195.27	148	79.69	0.7969
1	2.073	271.25	69.90	85.38	0.8538

Figure 5 depicts the equivalent circuit that determines TGETPT alloy and electrolyte. The EIS parameters are provided in Table 2. The divergence from the ideal semicircle was usually caused by frequency dispersion as well as surface inhomogeneity, grain boundaries, and contaminants. Increasing the TGETPT doses increases the charge transfer resistance

(R_{ct}) due to an increase in the thickness of the adsorbed layer and decreases the double layer capacitance (C_{dl}) due to the replacement of the adsorbed water molecules on the TGETPT surface by the inhibitor molecules, which confirms that the TGETPT particles function by adsorption at the TGETPT/interface [46].

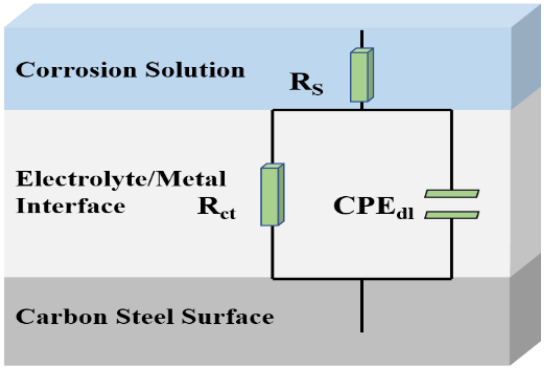

Figure 5. Equivalent electrical circuit of the E24 metal/TGETPT/1 M HCl.

3.3. Adsorption isotherm

The adsorption isotherm is used to investigate the mechanism of inhibitor adsorption. The adsorption process is affected by the electrical properties of the inhibitor, the surface nature of the metals, temperature, steric effects, and the different degrees of activity of a site [47]. Adsorption occurs as a result of interactions between active sites of molecules and the orbitals of steel atoms. Adsorption isotherm models such as Langmuir, Frumkin, Temkin, and Flory-Huggins are widely employed to evaluate the nature of these interactions [48].

According to the Langmuir isotherm, adsorption coefficient (θ) is related to the inhibitor concentration C_{inh} by the following equation [49, 50]:

$$\frac{C_{inh}}{\theta} = \frac{1}{K_{ads}} + C_{inh} \tag{5}$$

$$K_{ads} = \frac{1}{55.5} e^{-\left(\frac{\Delta G^0_{ads}}{RT}\right)} \tag{6}$$

where C_{inh}, K_{ads}, ΔG^0_{ads}, R and T are the concentration of TGETPT, surface coverage degree, free energy adsorption, constant of perfect gases and temperature, respectively.
The plot of C_{inh}/θ as a function of C_{inh} inhibitor concentration is linear (Figure 6), indicating that the product is adsorbing according to the Langmuir isotherm model

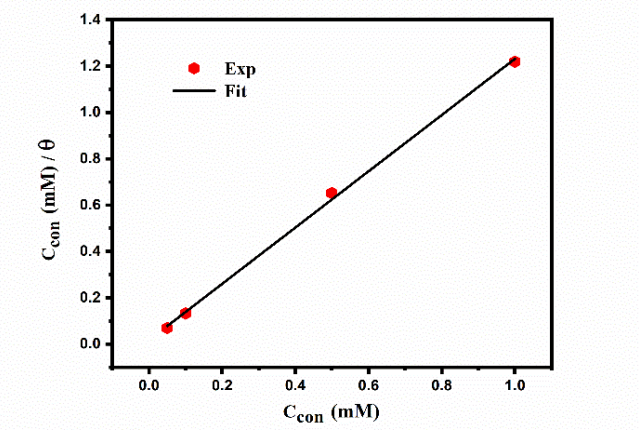

Figure 6. Langmuir adsorption isotherm of the TGETPT on the surface of the E24 carbon steel at 293 K.

Table 3. Parameters of adsorption of the TGETPT inhibitor.

Inhibitor	K **(mol^{-1}·L)**	R^2	ΔG^0_{ads} **(kJ·mol^{-1})**
TGETPT	56.47	0.99879	–19.96

The values of the free energy of adsorption of the TGETPT inhibitor are presented in Table 3. The ΔG^0_{ads} values obtained suggest that the electrostatic interactions between charged molecules and metal is a physical adsorption [51]. Also, the negative ΔG^0_{ads} indicates that the adsorption processes is spontaneous and the adsorbed layer is stable [53].

3.4. Temperature effect

In aggressive conditions and high temperatures, the stability of a corrosion inhibitor is essential. In addition, an increase in temperature would favour the desorption of the TGETPT inhibitor and the fast disintegration of the investigated epoxy polymer, thereby decreasing the corrosion resistance of carbon steel E24 [53]. The temperature effect on the change in the rates of corrosion and efficiency of the TGETPT at a concentration of 10^{-3} M within a temperature range of between 293 and 323 K are summarized in Table 4.

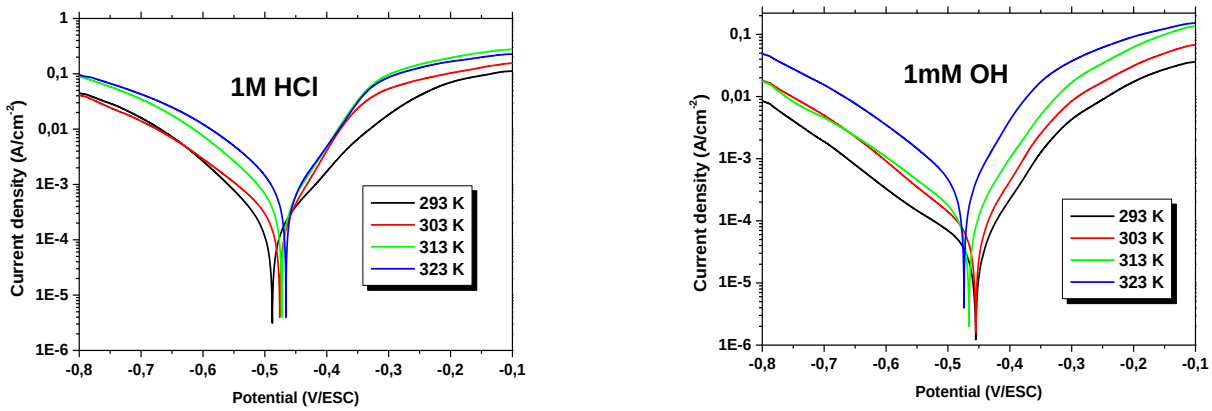

Figure 7. Polarization curves of E24 steel at various temperatures in 1 M HCl solution obtained (a) in the blank and (b) at 10^{-3} M of TGETPT.

Table 4. Corrosion current density and inhibitory efficiency at different temperatures for 1 mM of TGETPT.

[TGETPT] (mM)	*T* (K)	E_{corr} (mV/Ag–AgCl)	I_{corr} (μA/cm^2)	*IE*%
0	293	–488	174.8	
	303	–476	234.7	
	313	–473	341.7	
	323	–466	735.6	
1 mM	293	–455	24.37	86.06
	303	–455	59.64	74.58
	313	–466	98.92	71.05
	323	–474	235.7	67.96

3.5. Surface analysis

3.5.1. Scanning electron microscope (SEM)

The figure depicts a micrograph of the surface of the E24 steel submerged in 1 M HCl medium for 20 hours in the absence and in the presence of the TGETPT inhibitor.

In the absence of inhibitor, steel corrodes on the surface and an iron oxide layer was formed (grey spots in Figure 8a).

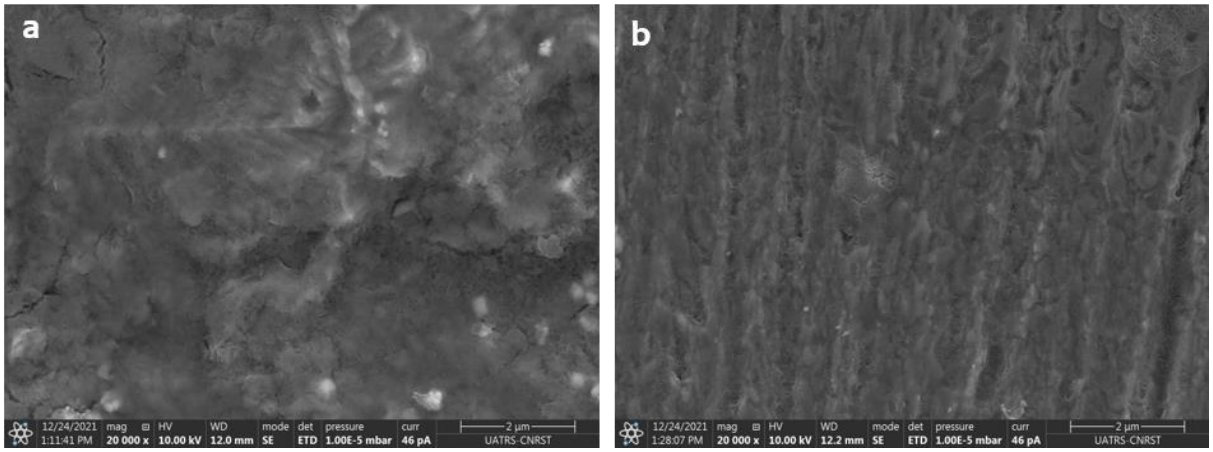

Figure 8. SEM image of E24 carbon steel after immersion for 20 h in 1 M HCl without (a) and with 1 mM of TGETPT (b).

With TGETPT added, a significant improvement in surface quality by the inhibitor protective coating was observed (Figure 8b).

3.5.2. EDX analysis

EDX analysis was used to identify the various elements present on the steel's surface. Figure 9 shows the EDX analysis of the E24 steel immersed in 1 M HCl for 20 hours, the oxygen and iron peaks in Figure 9a suggested an iron oxide compound [24].

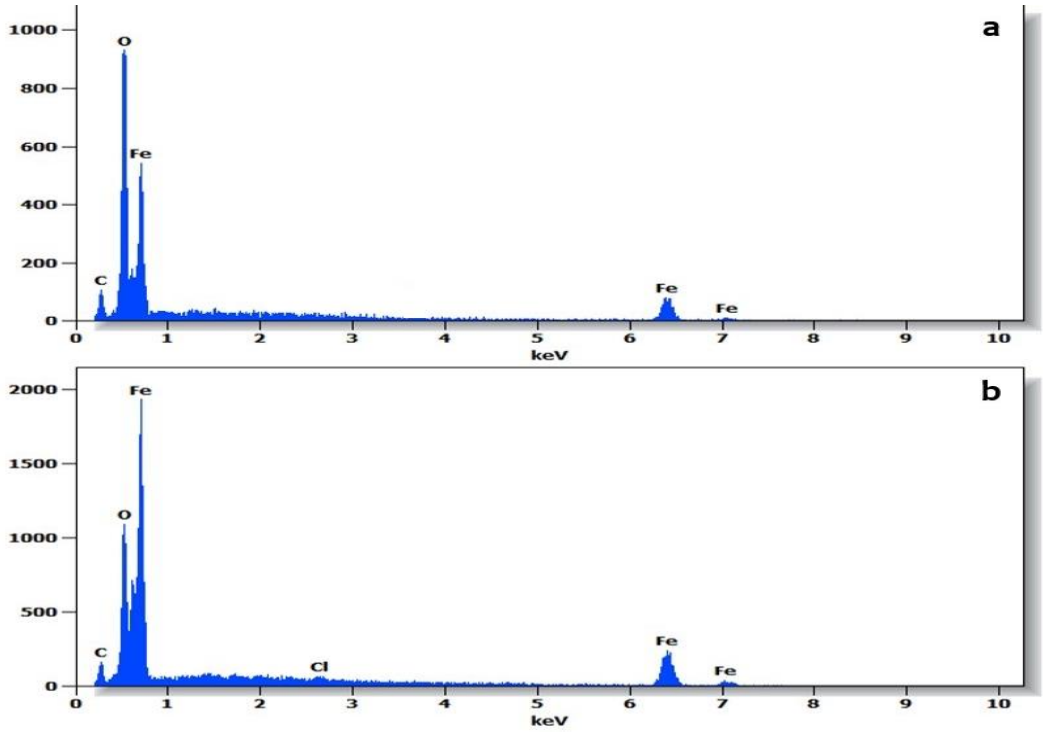

Figure 9. EDX of the state of the surface of mild steel immersed in 1M HCl for 20 hours of immersion: (a) in the absence of inhibitor (b) in the presence of 1 mM in TGETPT.

EDX analysis of the spectrum (Figure 9b) confirms the anti-corrosion character of TGETPT and results in the absence of the peak relating to the corrosion product (O, Fe). This result confirms that obtained by electrochemical methods and confirms that TGETPT reduces corrosion of E24 steel by forming a layer that limits the access of the electrolyte to the steel's surface.

3.6. DFT results

That the electronic structure of an inhibitor molecule is related to its corrosion prevention capacity, and it has been reported that some molecular electronic parameters have been correlated to inhibition efficiency [54]. Table 5 summarizes some relevant electronic parameters, namely energies of highest occupied and lowest unoccupied molecular orbitals (E_{HOMO} and E_{LUMO}, respectively), energy gap ($\Delta E_{LUMO-HOMO}$), hardness (η), and electronegativity (χ) of inhibitor molecule, as well as a fraction of transferred electrons (ΔN) and initial inhibitor/surface interaction energy (ΔE_i) of inhibitor with the iron surface.

According to the frontier molecular orbital theory, a molecule with higher E_{HOMO} and lower E_{LUMO}, which implies a small energy gap, can exhibit more tendency to be a reactive specie, *i.e.* a softer molecule (low η) [55]. Consequently and in the light of obtained results, the tested compound exhibits a small energy gap (4.310 eV) and hardness (2.155 eV) values that explain the highest prevention efficiency recorded in the current work. It is interesting to know that similar values have been reported elsewhere for many effective heterocyclic-based corrosion inhibitors [56, 57]. To consider implicitly the role of surface and intrinsic electronic properties of the inhibitor (η and χ) in the adsorption process, the ΔN parameter is often used [32]. The ability of a given inhibitor to transfer electrons to the metal surface is characterized by $\Delta N>0$, whereas the inverse trend is observed if $\Delta N<0$. In our case, the obtained value (0.250 e) outlines the ability of the tested inhibitor to donate electrons to the metal surface, which leads to its effective adsorption and then the formation of a protective film on the surface. ΔE_i is another parameter employs to expect implicitly the interfacial interactions between the inhibitor molecule and the target metal [58]. The negative sign (−0.134 eV) of calculated ΔE_i reveals the exothermic character of the interaction, as well as its spontaneous nature, of the investigated inhibitor with the iron metal. These findings demonstrate the accurate affinity of the used inhibitor to adsorb into the metal surface, which is in good agreement with experimental achievements.

Table 5. Molecular electronic parameters of investigated inhibitor calculated by GGA/BLYP method with DNP 3.6 basis set.

E_{HOMO} (eV)	E_{LUMO} (eV)	$\Delta E_{LUMO-HOMO}$ (eV)	H (eV)	χ (eV)	ΔN (e)	ΔE_i (eV)
–5.899	–1.589	4.310	2.155	3.744	0.250	–0.134

To explore the active centers by which inhibitor can adsorb onto the metal surface, the electrostatic potential (ESP) map and distribution of frontier molecular orbitals are computed and are shown at the 0.02-isosurface value in Figure 10.

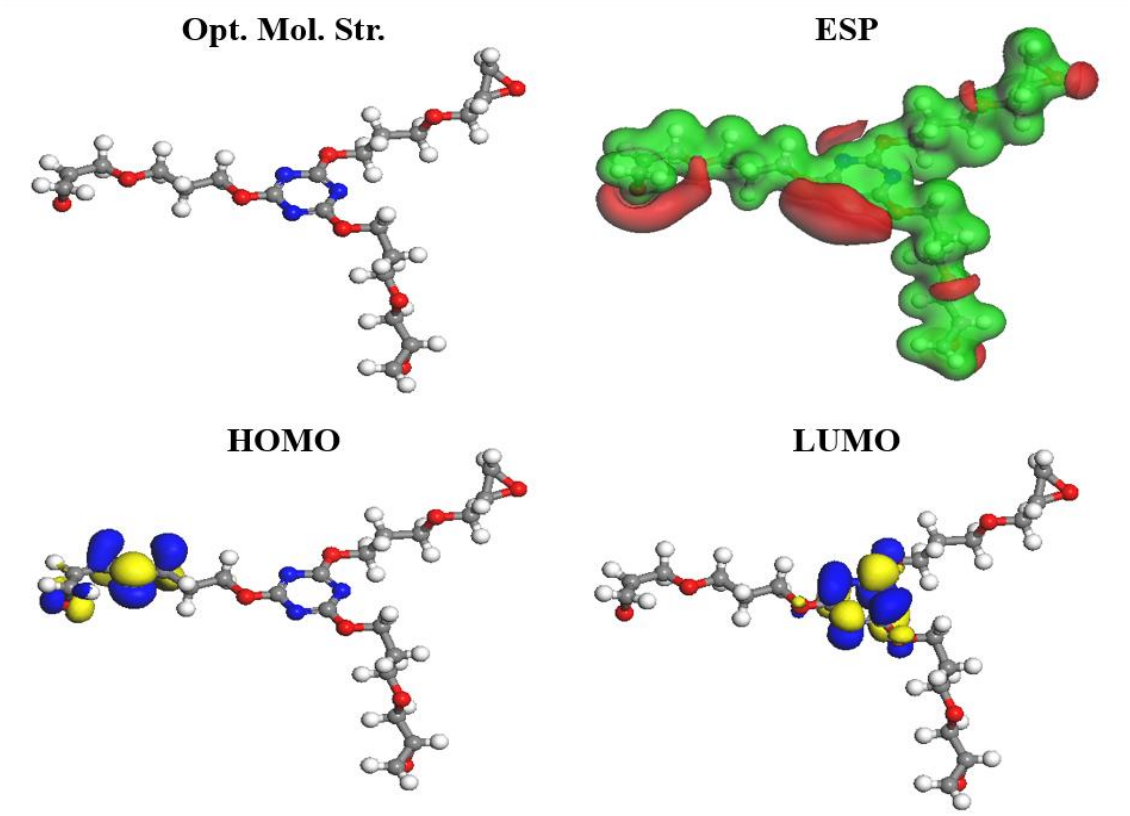

Figure 10. Optimized molecular structure, ESP map (red and green colors refer to electronegative and electropositive potentials, respectively) and frontier molecular orbitals (HOMO and LUMO) of tested inhibitor.

The ESP map is widely served to shed light on the favourable regions of inhibitor by which it can adsorb electrostatically onto the metal surface [32]. According to the obtained ESP map, negative potentials (*i.e.*, electron-rich regions) are located on almost heteroatoms of inhibitor, whereas the rest of inhibitor molecule is characterized by positive potentials (*i.e.*, electron-poor regions). This finding can be also confirmed based on the atomic charges as tabulated in Table 6. It is recognized that the metal surface is an electron-poor system; consequently, the inhibitor molecule can interact favourably with the surface via those electron-rich sites [59].

Moreover, as these sites are speared homogeny over the inhibitor skeleton, parallel adsorption onto the surface is expected. Such adsorption configuration can provide accurate surface coverage, which leads to enhanced protection performance. On the other hand, among the three side substituents of the ring, it was found that HOMO lobes are located on one extra substituent (Figure 10). This means that the inhibitor tends to share electrons with the metallic surface probably through this region of the inhibitor molecule [60]. A different

distribution is observed in the case of LUMO orbitals, which are more concentrated on the ring. This lets us expect if there is an acceptance of electrons by the inhibitor from the metal surface, this will occur favourably on the ring [56].

Table 6. Atomic charges of inhibitor molecule according to Mulliken population analysis.

Atom	Charge	Atom	Charge	Atom	Charge
N (1)	–0.465	C (12)	0.183	O (23)	–0.542
C (2)	0.559	C (13)	0.166	C (24)	0.120
N (3)	–0.466	C (14)	0.120	O (25)	–0.488
C (4)	0.56	O (15)	–0.542	C (26)	0.169
N (5)	–0.463	O (16)	–0.488	C (27)	–0.108
C (6)	0.544	C (17)	0.143	C (28)	0.184
O (7)	–0.490	C (18)	–0.103	O (29)	–0.565
C (8)	0.160	C (19)	0.182	C (30)	0.185
C (9)	–0.117	O (20)	–0.568	C (31)	0.171
C (10)	0.178	C (21)	0.184	C (32)	0.110
O (11)	–0.567	C (22)	0.167	O (33)	–0.553

3.7. Dynamic molecular findings

It is well known that the modeling of inhibitor surface interactions is a rigorous approach in corrosion inhibition investigations [58]. In this regard, the interfacial interaction between the tested inhibitor and metal surface was studied using a dynamic molecular simulation tool under the solvation effect at 298 K. As can be seen from Figure 11, the inhibitor exhibits a noticeable tendency to adsorb onto the target metal, which is closely placed to the surface. Moreover, the inhibitor shows a parallel adsorption orientation vis Fe(110) surface, which leads to maximizing the surface coverage of the metal surface [61]. Such an adsorption configuration can be related to the homogeneous distribution of the favourable adsorption centers within the molecular skeleton of inhibitor, which are involved in these interfacial interactions with the iron surface [62]. On the other hand, to examine the stability of obtained adsorption system, the adsorption energy is calculated. It was found to be equal to $-296.823\ \text{kcal}\cdot\text{mol}^{-1}$, the negative sign of obtained energy value outlines the spontaneous behavior of inhibitor adsorption onto the Fe(110) surface [63]. Moreover, the magnitude of adsorption energy is interesting, which outlines the stability of the studied inhibitor/metal system. This signifies strong adsorption of investigated inhibitor onto the iron surface, which implies the formation of a more adherent protective film on the metal surface [64, 65]. Similar adsorption energy has been reported for many efficient corrosion inhibitors in the

literature [66, 67]. These results support and explain the good prevention ability of investigated inhibitor for mild steel in hydrochloride solution.

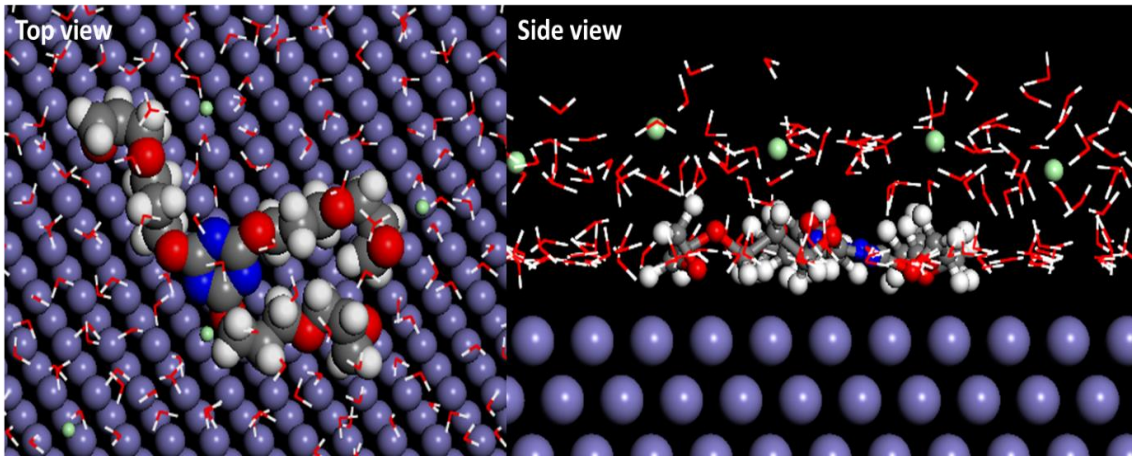

Figure 11. Top and side snapshots of equilibrium adsorption configuration of inhibitor on Fe(110) surface under solvation condition.

4. Conclusion

The impact of TGETPT on the corrosion of E24 carbon steel in 10^{-3} M HCl solution was investigated utilizing electrochemical techniques such as polarization curves and electrochemical impedance spectroscopy. The following conclusions may be drawn from this study:

- TGETPT is rather good corrosion inhibitor, with an effectiveness of 81.6% at 10^{-3} M concentration. The polarization curves showed a decrease in the density of corrosion currents as a function of the concentration of TGETPT.
- The amplitude of the impedance diagrams is affected by the variation of the concentration. Indeed, as the concentration and charge transfer resistor load increase, so does the size of the capacitive loop. On the other hand, the capacity decreases for the inhibitor tested.
- The influence of temperature on steel corrosion behavior and inhibitory efficiency was investigated in a temperature range of 293 K to 323 K, revealing an increase in corrosion rate and a decrease in TGETPT efficiency.
- Electronic and atomic analysis of the inhibitor based on DFT calculations and molecular dynamic simulations, respectively, support and justify its ability to act as a potent anti-corrosion agent for mild steel in an acidic medium.

References

1. O.R. Adetunji, O.O. Ude, S.I. Kuye, E.O. Dare, K.O. Alamu and S.A. Afolalu, Potentiodynamic Polarization of Brass, Stainless and Coated Mild Steel in 1M Sodium Chloride Solution, *Int. J. Eng. Res. Afr.*, 2016, **23**, no. 2, 1–7. doi: 10.4028/www.scientific.net/JERA.23.1

2. M. Benarioua, A. Mihi, N. Bouzeghaia and M. Naoun, Mild steel corrosion inhibition by Parsley (Petroselium Sativum) extract in acidic media, *Egypt. J. Pet*., 2019, **28**, no. 2, 155–159. doi: 10.1016/j.ejpe.2019.01.001
3. C. Verma, E.E. Ebenso, I. Bahadur and M. A. Quraishi, An overview on plant extracts as environmental sustainable and green corrosion inhibitors for metals and alloys in aggressive corrosive media, *J. Mol. Liq*., 2018, **266**, 577–590. doi: 10.1016/j.molliq.2018.06.110
4. W. Belmaghraoui, A. Mazkour, H. Harhar, M. Harir and S. El Hajjaji, Investigation of corrosion inhibition of C38 steel in 5.5 M H_3PO_4 solution using *Ziziphus* lotus oil extract: an application model, *Anti-Corros. Methods Mater*., 2018, **66**, no. 1, 121–126. doi: 10.1108/ACMM-02-2018-1901
5. C.M. Hansson, The Impact of Corrosion on Society, *Metall. Mater. Trans*. A, 2011, **42**, no. 10, 2952–2962. doi: 10.1007/s11661-011-0703-2
6. F. Bouhlal, A. Mazkour, H. Labjar, M. Benmessaoud, M. Serghini-Idrissi, M. El Mahi, S. El Hajjaji and N. Labjar, Combination effect of hydro-alcoholic extract of spent coffee grounds (HECG) and potassium Iodide (KI) on the C38 steel corrosion inhibition in 1 M HCl medium: Experimental design by response surface methodology, *Chem. Data Collect*., 2020, **29**, 100499.
7. M. Damej, A. Molhi, H. Lgaz, R. Hsissou, J. Aslam, M. Benmessaoud, N. Rezki, H.S. Lee and D.E. Lee, Performance and interaction mechanism of a new highly efficient benzimidazole-based epoxy resin for corrosion inhibition of carbon steel in HCl: A study based on experimental and first-principles DFTB simulations, *J. Mol. Struct*., 2023, **1273**, 134232. doi: 10.1016/j.molstruc.2022.134232
8. K. Azgaou, M. Damej, S. El Hajjaji, N.K. Sebbar, H. Elmsellem, B. El Ibrahimi and M. Benmessaoud, Synthesis and characterization of *N*-(2-aminophenyl)-2-(5-methyl-1*H*-pyrazol-3-yl) acetamide (AMPA) and its use as a corrosion inhibitor for C38 steel in 1 M HCl. Experimental and theoretical study, *J. Mol. Struct*., 2022, **1266**, 133451. doi: 10.1016/j.molstruc.2022.133451
9. Y. El Hamdouni, F. Bouhlal, H. Kouri, M. Chellouli, M. Benmessaoud, A. Dahrouch, N. Labjar and S. El Hajjaji, Use of Omeprazole as Inhibitor for C38 Steel Corrosion in 1.0 M H_3PO_4 Medium, *J. Fail. Anal. and Preven*., 2020, **20**, no. 2, 563–571. doi: 10.1007/s11668-020-00862-5
10. P.P. Kumari, P. Shetty and S.A. Rao, Electrochemical measurements for the corrosion inhibition of mild steel in 1 M hydrochloric acid by using an aromatic hydrazide derivative, *Arabian J. Chem*., 2017, **10**, no. 5, 653–663. doi: 10.1016/j.arabjc.2014.09.005
11. C. Verma, M.A. Quraishi, L.O. Olasunkanmi and E.E. Ebenso, l-Proline-promoted synthesis of 2-amino-4-arylquinoline-3-carbonitriles as sustainable corrosion inhibitors for mild steel in 1 M HCl: experimental and computational studies, *RSC Adv*., 2015, **5**, no. 104, 85417–85430. doi: 10.1039/C5RA16982H

12. N. Chaubey, Savita, V.K. Singh and M.A. Quraishi, Corrosion inhibition performance of different bark extracts on aluminium in alkaline solution, *J. Assoc. Arab Univ. Basic Appl. Sci*., 2017, **22**, no. 1, 38–44. doi: 10.1016/j.jaubas.2015.12.003
13. B.O. Abdelwedoud, M. Damej, K. Tassaoui, A. Berishab, H. Tachallait, K. Bougrin, V. Mehmeti and M. Benmessaoud, Inhibition effect of N-propargyl saccharin as corrosion inhibitor of C38 steel in 1 M HCl, experimental and theoretical study, *J. Mol. Liq*., 2022, **354**, 118784.
14. M. Damej, R. Hsissou, A. Berisha, K. Azgaou, M. Sadiku, M. Benmessaoud, N. Labjar, S. El Hajjaji, New epoxy resin as a corrosion inhibitor for the protection of carbon steel C38 in 1 M HCl. experimental and theoretical studies (DFT, MC, and MD), *J. Mol. Struct*., 2022, **1254**, 132425. doi: 10.1016/j.molstruc.2022.132425
15. M. Damej, A. Molhi, K. Tassaoui, B. El Ibrahimi, Z. Akounach, A.A. Addi, S. El Hajjaji and M. Benmessaoud, Experimental and Theoretical Study to Understand the Adsorption Process of p-Anisidine and 4-Nitroaniline for the Dissolution of C38 Carbon Steel in 1 M HCl, *ChemistrySelect*, 2022, **7**, no. 2. doi: 10.1002/slct.202103192
16. H.A. Al-Sharabi, F. Bouhlal, K. Bouiti, N. Labjar, E. Al Zalaei, A. Dahrouch, G.A. Benabdellah, M. El Mahi, M. Benmessaoud, E.M. Lotfi, B. El Otmani and S. El Hajjaji, Electrochemical and thermodynamic evaluation on corrosion inhibition of C38 steel in 1 M HCl by Rumex ethanolic extract, *Int. J. Corros. Scale Inhib*., 2022, **11**, no. 1, 382–401. doi: 10.17675/2305-6894-2022-11-1-23
17. A. Molhi, R. Hsissou, M. Damej, A. Berisha, M. Bamaarouf, M. Seydou, M. Benmessaoud and S. El Hajjaji, Performance of two epoxy compounds against corrosion of C38 steel in 1 M HCl: Electrochemical, thermodynamic and theoretical assessment, *Int. J. Corros. Scale Inhib*., 2021, **10**, no. 2, 812–837. doi: 10.17675/2305-6894-2021-10-2-21
18. A. Molhi, R. Hsissou, M. Damej, A. Berisha, V. Thaçi, A. Belafhaili, M. Benmessaoud, N. Labjar and S. El Hajjaji, Contribution to the corrosion inhibition of c38 steel in 1 m hydrochloric acid medium by a new epoxy resin PGEPPP, *Int. J. Corros. Scale Inhib*., 2021, **10**, no. 1, 399–418. doi: 10.17675/2305-6894-2021-10-1-23
19. K. Chkirate, K. Azgaou, H. Elmsellem, B. El Ibrahimi, N.K. Sebbar, El H. Anouar, M. Benmessaoud, S. El Hajjaji and El M. Essassi, Corrosion inhibition potential of 2-[(5-methylpyrazol-3-yl)methyl]benzimidazole against carbon steel corrosion in 1 M HCl solution: Combining experimental and theoretical studies, *J. Mol. Liq*., 2021, **321**, 114750. doi: 10.1016/j.molliq.2020.114750
20. Al Maofari, S. Douch, M. Benmessaoud, B. Ouaki, M. Mosaddak and S. El Hajjaji, Inhibition study of various extracts of tribulus terrestris plant on the corrosion of mild steel in a 1.0 M HCl solution, *Port. Electrochim. Acta*, 2021, **39**, no. 1, 21–35.

21. H. Lgaz, S. Masroor, M. Chafiq, M. Damej, A. Brahmia, R. Salghi, M. Benmessaoud, I.H. Ali, M.M. Alghamdi, A. Chaouiki and Ill-Min Chung, Evaluation of 2-mercaptobenzimidazole derivatives as corrosion inhibitors for mild steel in hydrochloric acid, *Metals*, 2020, **10**, no. 3, 357. doi: 10.3390/met10030357
22. Z. Akounach, A. Al Maofari, A. El Yadini, S. Douche, M. Benmessaoud, B. Ouaki, M. Damej and S.E.L. Hajjaji, Inhibition of mild steel corrosion in 1.0 M HCl by water, hexane and ethanol extracts of pimpinella anisum plant, *Anal. Bioanal. Electrochem.*, 2018, **10**, no. 11, 1506–1524.
23. Z. Lakbaibi, M. Damej, A. Molhi, M. Benmessaoud, S. Tighadouini, A. Jaafar, T. Benabbouha, A. Ansari, A. Driouich and M. Tabyaoui, Evaluation of inhibitive corrosion potential of symmetrical hydrazine derivatives containing nitrophenyl moiety in 1 M HCl for C38 steel: experimental and theoretical studies, *Heliyon*, 2022, **8**, no. 3, e09087. doi: 10.1016/j.heliyon.2022.e09087
24. M. Damej, S. Kaya, B. El Ibrahimi, H.S. Lee, A. Molhi, G. Serdaroğlu, M. Benmessaoud. I.H Ali, S. El Hajjaji, H. Lgaz, The corrosion inhibition and adsorption behavior of mercaptobenzimidazole and bis-mercaptobenzimidazole on carbon steel in 1.0 M HCl: Experimental and computational insights, *Surf. Interfaces*, 2021, **24**, 101095.
25. M. Chafiq, A. Chaouiki, M. Damej, H. Lgaz, R. Salghi, I.H. Ali, M. Benmessaoud, S. Masroor and Ill-Min Chung, Bolaamphiphile-class surfactants as corrosion inhibitor model compounds against acid corrosion of mild steel, *J. Mol. Liq.*, 2020, **309**, 113070. doi: 10.1016/j.molliq.2020.113070
26. R. Hsissou, R. Lachhab, A. El Magri, S. Echihi, H.R. Vanaei, M. Galai, M. Ebn Touhami and M. Rafik, Synthesis Characterization and Highly Protective Efficiency of Tetraglycidyloxy Pentanal Epoxy Prepolymer as a Potential Corrosion Inhibitor for Mild Steel in 1 M HCl Medium, *Polymers*, 2022, **14**, no. 15. doi: 10.3390/polym14153100
27. R. Hsissou, F. Benhiba, M. El Aboubi, S. Abbout, Z. Benzekri, Z. Safi, M. Rafik, H. Bahaj, M. Kaba, M. Galai, N. Wazzan, S. Briche, S. Boukhris, A. Zarrouk, M. EbnTouhami and M. Rafik, Synthesis and performance of two ecofriendly epoxy resins as a highly efficient corrosion inhibition for carbon steel in 1 M HCl solution: DFT, RDF, FFV and MD approaches, *Chem. Phys. Lett.*, 2022, **806**, 139995. doi: 10.1016/j.cplett.2022.139995
28. Z. Akounach, A. Al Maofari, M. Damej, S. El Hajjaji, A. Berisha, V. Mehmeti, N. Labjar, M. Bamaarouf and M. Benmessaoud, Contribution to the corrosion inhibition of aluminum in 1 M HCl by *Pimpinella Anisum* extract. Experimental and theoretical studies (DFT, MC, and MD), *Int. J. Corros. Scale Inhib.*, 2022, **11**, no. 1, 402–424. doi: 10.17675/2305-6894-2022-11-1-24

29. K. Tassaoui, M. Damej, A. Molhi, A. Berisha, M. Errili, S. Ksama, V. Mehmeti, S. El Hajjaji and M. Benmessaoud, Contribution to the corrosion inhibition of Cu–30Ni copper–nickel alloy by 3-amino-1,2,4-triazole-5-thiol (ATT) in 3% NaCl solution. Experimental and theoretical study (DFT, MC and MD), *Int. J. Corros. Scale Inhib*., 2022, **11**, no. 1, 221–244. doi: 10.17675/2305-6894-2022-11-1-12
30. D.A. López, W.H. Schreiner, S.R. de Sánchez and S.N. Simison, The influence of carbon steel microstructure on corrosion layers: An XPS and SEM characterization, *Appl. Surf. Sci*., 2003, **207**, no. 1–4, 69–85. doi: 10.1016/S0169-4332(02)01218-7
31. S. Hong, W. Chen, Y. Zhang, H.Q. Luo, M. Li and N.B. Li, Investigation of the inhibition effect of trithiocyanuric acid on corrosion of copper in 3.0wt.% NaCl, *Corros. Sci*., 2013, **66**, 308–314. doi: 10.1016/j.corsci.2012.09.034
32. K. Abderrahim, I. Selatnia, A. Sid and P. Mosset, 1,2-bis(4-chlorobenzylidene)Azine as new and effective corrosion inhibitor for copper in 0.1 N HCl: A combined experimental and theoretical approach, *Chem. Phys. Lett*., 2018, **707**, 117–128. doi: 10.1016/j.cplett.2018.07.046
33. H. Bourzi, R. Oukhrib, B. El Ibrahimi, H.A. Oualid, Y. Abdellaoui, B. Balkard, S. El Issami, M. Hilali, L. Bazzi and C. Len, Furfural Analogs as Sustainable Corrosion Inhibitors–Predictive Efficiency Using DFT and Monte Carlo Simulations on the Cu(111), Fe(110), Al(111) and Sn(111) Surfaces in Acid Media, Sustainability, 2020, **12**, no. 8, 3304. doi: 10.3390/su12083304
34. B. El Ibrahimi, A. Jmiai, K. El Mouaden, R. Oukhrib, A. Soumoue, S. El Issami and L. Bazzi, Theoretical evaluation of some α-amino acids for corrosion inhibition of copper in acidic medium: DFT calculations, Monte Carlo simulations and QSPR studies, *J. King Saud Univ., Sci*., 2020, **32**, no. 1, 163–171. doi: 10.1016/j.jksus.2018.04.004
35. B.E. Ibrahimi, L. Bazzi and S.E. Issami, The role of pH in corrosion inhibition of tin using the proline amino acid: theoretical and experimental investigations, *RSC Adv*., 2020, **10**, no. 50, 29696–29704. doi: 10.1039/D0RA04333H
36. B. El Ibrahimi, Atomic-scale investigation onto the inhibition process of three 1,5-benzodiazepin-2-one derivatives against iron corrosion in acidic environment, *Colloid Interface Sci. Commun*., 2020, **37**, 100279. doi: 10.1016/j.colcom.2020.100279
37. X. Li, S. Deng and X. Xie, Experimental and theoretical study on corrosion inhibition of oxime compounds for aluminium in HCl solution, *Corros. Sci*., 2014, **81**, 162–175. doi: 10.1016/j.corsci.2013.12.021
38. V.V. Torres, R.S. Amado, C.F. de Sá, T.L. Fernandez, C.A. da Silva Riehl, A.G. Torres and E. D'Elia, Inhibitory action of aqueous coffee ground extracts on the corrosion of carbon steel in HCl solution, *Corros. Sci*., 2011, **53**, no. 7, 2385–2392. doi: 10.1016/j.corsci.2011.03.021
39. E.S. Ferreira, C. Giacomelli, F.C. Giacomelli and A. Spinelli, Evaluation of the inhibitor effect of l-ascorbic acid on the corrosion of mild steel, *Mater. Chem. Phys*., 2004, **83**, no. 1, 129–134. doi: 10.1016/j.matchemphys.2003.09.020

40. M. Abdallah, Rhodanine azosulpha drugs as corrosion inhibitors for corrosion of 304 stainless steel in hydrochloric acid solution, *Corros. Sci*., 2002, **44**, no. 4, 717–728. doi: 10.1016/S0010-938X(01)00100-7
41. I. Ahamad, R. Prasad and M.A. Quraishi, Adsorption and inhibitive properties of some new Mannich bases of Isatin derivatives on corrosion of mild steel in acidic media, *Corros. Sci*., 2010, **52**, no. 4, 1472–1481. doi: 10.1016/j.corsci.2010.01.015
42. J.O. Bockris and S. Srinivasan, Elucidation of the mechanism of electrolytic hydrogen evolution by the use of H-T separation factors, *Electrochim. Acta*, 1964, **9**, no. 1, 31–44. doi: 10.1016/0013-4686(64)80003-7
43. G. Bahlakeh, A. Dehghani, B. Ramezanzadeh and M. Ramezanzadeh, Highly effective mild steel corrosion inhibition in 1 M HCl solution by novel green aqueous *Mustard* seed extract: Experimental, electronic-scale DFT and atomic-scale MC/MD explorations, *J. Mol. Liq*., 2019, **293**, 111559. doi: 10.1016/j.molliq.2019.111559
44. H. Ashassi-Sorkhabi, B. Shaabani and D. Seifzadeh, Corrosion inhibition of mild steel by some schiff base compounds in hydrochloric acid, *Appl. Surf. Sci*., 2005, **239**, no. 2, 154–164. doi: 10.1016/j.apsusc.2004.05.143
45. A. Dehghani, G. Bahlakeh, B. Ramezanzadeh and M. Ramezanzadeh, A combined experimental and theoretical study of green corrosion inhibition of mild steel in HCl solution by aqueous *Citrullus lanatus* fruit (CLF) extract, *J. Mol. Liq*., 2019, **279**, 603–624. doi: 10.1016/j.molliq.2019.02.010
46. R.A.H. Al-Uqaily and S.A. Al-Bayaty, Study A Corrosion Inhibitor Of 1-Isoquinolinyl Phenyl Ketone For Mild Steel In Acidic Medium As Hcl Acid, *J. Phys.: Conf. Ser*., 2019, **1294**, no. 5, 052014. doi: 10.1088/1742-6596/1294/5/052014
47. Y. Feng, S. Chen, W. Guo, Y. Zhang and G. Liu, Inhibition of iron corrosion by 5,10,15,20-tetraphenylporphyrin and 5,10,15,20-tetra-(4-chlorophenyl)porphyrin adlayers in 0.5 M H_2SO_4 solutions, *J. Electroanal. Chem*., 2007, **602**, no. 1, 115–122. doi: 10.1016/j.jelechem.2006.12.016
48. I.B. Obot, D.D. Macdonald and Z.M. Gasem, Density functional theory (DFT) as a powerful tool for designing new organic corrosion inhibitors. Part 1: An overview, *Corros. Sci*., 2015, **99**, 1–30. doi: 10.1016/j.corsci.2015.01.037
49. M. Damej, H. Benassaoui, D. Chebabe, M. Benmessaoud, H. Erramli, A. Dermaj, N. Hajjaji and A. Srhiri, Inhibition effect of 1,2,4-triazole-5-thione derivative on the Corrosion of Brass in 3% NaCl solution, *J. Mater. Environ. Sci*., 2016, 7, no. 3, 738–745.
50. R. Hsissou, F. Benhiba, S. Abbout, O. Dagdag, S. Benkhaya, A. Berisha, H. Erramli and A. Elharfi, Trifunctional epoxy polymer as corrosion inhibition material for carbon steel in 1.0 M HCl: MD simulations, DFT and complexation computations, *Inorg. Chem. Commun*., 2020, **115**, 107858. doi: 10.1016/j.inoche.2020.107858

51. M. Behpour, S.M. Ghoreishi, N. Soltani, M. Salavati-Niasari, M. Hamadanian and A. Gandomi, Electrochemical and theoretical investigation on the corrosion inhibition of mild steel by thiosalicylaldehyde derivatives in hydrochloric acid solution, *Corros. Sci*., 2008, **50**, no. 8, 2172–2181. doi: 10.1016/j.corsci.2008.06.020
52. F. Bentiss, M. Lebrini and M. Lagrenée, Thermodynamic characterization of metal dissolution and inhibitor adsorption processes in mild steel/2,5-bis(n-thienyl)-1,3,4-thiadiazoles/hydrochloric acid system, *Corros. Sci*., 2005, **47**, no. 12, 2915–2931. doi: 10.1016/j.corsci.2005.05.034
53. Z. Rouifi, F. Benhiba, M. El Faydy, T. Laabaissi, H. About, H. Oudda, I. Warad, A. Guenbour, B. Lakhrissi and A. Zarrouk, Performance and computational studies of new soluble triazole as corrosion inhibitor for carbon steel in HCl, *Chem. Data Collect*., 2019, **22**, 100242. doi: 10.1016/j.cdc.2019.100242
54. Z. Cao, Y. Tang, H. Cang, J. Xu, G. Lu and W. Jing, Novel benzimidazole derivatives as corrosion inhibitors of mild steel in the acidic media. Part II: Theoretical studies, *Corros. Sci*., 2014, **83**, 292–298. doi: 10.1016/j.corsci.2014.02.025
55. C. Verma, L.O. Olasunkanmi, E.E. Ebenso and M.A. Quraishi, Adsorption characteristics of green 5-arylaminomethylene pyrimidine-2,4,6-triones on mild steel surface in acidic medium: Experimental and computational approach, *Results Phys*., 2018, **8**, 657–670. doi: 10.1016/j.rinp.2018.01.008
56. L.O. Olasunkanmi, M.E. Mashuga and E.E. Ebenso, Surface protection activities of some 6-substituted 3-chloropyridazine derivatives for mild steel in 1 M hydrochloric acid: Experimental and theoretical studies, Surf. Interfaces, 2018, **12**, 8–19. doi: 10.1016/j.surfin.2018.04.003
57. S. John, A. Joseph, T. Sajini and A.J. Jose, Corrosion inhibition properties of 1,2,4-Hetrocyclic Systems: Electrochemical, theoretical and Monte Carlo simulation studies, *Egypt. J. Pet*., 2017, **26**, no. 3, 721–732. doi: 10.1016/j.ejpe.2016.10.005
58. A. Kokalj, Is the analysis of molecular electronic structure of corrosion inhibitors sufficient to predict the trend of their inhibition performance, *Electrochim. Acta*, 2010, **56**, no. 2, 745–755. doi: 10.1016/j.electacta.2010.09.065
59. K.R. Ansari, D.S. Chauhan, M.A. Quraishi, M.A.J. Mazumder and A. Singh, Chitosan Schiff base: an environmentally benign biological macromolecule as a new corrosion inhibitor for oil & gas industries, *Int. J. Biol. Macromol*., 2020, **144**, 305–315. doi: 10.1016/j.ijbiomac.2019.12.106
60. A. Singh, K.R. Ansari, Y. Lin, M.A. Quraishi, H. Lgaz and I.-M. Chung, Corrosion inhibition performance of imidazolidine derivatives for J55 pipeline steel in acidic oilfield formation water: Electrochemical, surface and theoretical studies, *J. Taiwan Inst. Chem. Eng*., 2019, **95**, 341–356. doi: 10.1016/j.jtice.2018.07.030

61. B. El Ibrahimi, A. Baddouh, R. Oukhrib, S. El Issami, Z. Hafidi and L. Bazzi, Electrochemical and in silico investigations into the corrosion inhibition of cyclic amino acids on tin metal in the saline environment, *Surf. Interfaces*, 2021, **23**, 100966. doi: 10.1016/j.surfin.2021.100966
62. R. Oukhrib, B. El Ibrahimi, H.A. Oualid, Y. Abdellaoui, S. El Issami, L. Bazzi, M. Hilali and H. Bourzi, In silico investigations of alginate biopolymer on the Fe (110), Cu (111), Al (111) and Sn (001) surfaces in acidic media: Quantum chemical and molecular mechanic calculations, *J. Mol. Liq*., 2020, **312**, 113479. doi: 10.1016/j.molliq.2020.113479
63. L.H. Madkour, S. Kaya, L. Guo and C. Kaya, Quantum chemical calculations, molecular dynamic (MD) simulations and experimental studies of using some azo dyes as corrosion inhibitors for iron. Part 2: Bis-azo dye derivatives, *J. Mol. Struct*., 2018, **1163**, 397–417. doi: 10.1016/j.molstruc.2018.03.013
64. A. Kokalj, H. Behzadi and R. Farahati, DFT study of aqueous-phase adsorption of cysteine and penicillamine on Fe(110): Role of bond-breaking upon adsorption, *Appl. Surf. Sci*., 2020, **514**, 145896. doi: 10.1016/j.apsusc.2020.145896
65. H. Bourzi, R. Oukhrib, B. El Ibrahimi, H.A. Oualid, Y. Abdellaoui, B. Balkard, M. Hilali and S. El Issami, Understanding of anti-corrosive behavior of some tetrazole derivatives in acidic medium: Adsorption on Cu (111) surface using quantum chemical calculations and Monte Carlo simulations, *Surf. Sci*., 2020, **702**, 121692. doi: 10.1016/j.susc.2020.121692
66. C. Verma, L.O. Olasunkanmi, E.E. Ebenso, M.A. Quraishi and I.B. Obot, Adsorption Behavior of Glucosamine-Based, Pyrimidine-Fused Heterocycles as Green Corrosion Inhibitors for Mild Steel: Experimental and Theoretical Studies, *J. Phys. Chem. C*, 2016, **120**, no. 21, 11598–11611. doi: 10.1021/acs.jpcc.6b04429
67. F. Zhang, Y. Tang, Z. Cao, W. Jing, Z. Wu and Y. Chen, Performance and theoretical study on corrosion inhibition of 2-(4-pyridyl)-benzimidazole for mild steel in hydrochloric acid, *Corros. Sci*., 2012, **61**, 1–9. doi: 10.1016/j.corsci.2012.03.045

♦ ♦ ♦